Respective roles of scatter, attenuation, depth-dependent collimator response and finite spatial resolution in cardiac single-photon emission tomography quantitation: a Monte Carlo study

Georges N. El Fakhri[1], Irène Buvat[1], Mélanie Pélégrini[1], Habib Benali[1], Pedro Almeida[2], Bernard Bendriem[2], Andrew Todd-Pokropek[1], Robert Di Paola[1]

[1] U494 INSERM, CHU Pitié-Salpêtrière, 91 Boulevard de l'Hôpital, F-75634 Paris cedex 13, France
[2] SHFJ, Groupe instrumentation PET/SPET, 4 Place du Général Leclerc, F-91401 Orsay cedex, France

Abstract. The purpose of this study was to investigate the relative influence of scatter, attenuation, depth-dependent collimator response and finite spatial resolution upon the image characteristics in cardiac single-photon emission tomography (SPET). An acquisition of an anthropomorphic cardiac phantom was performed together with corresponding SPET Monte Carlo simulations. The cardiac phantom and the Monte Carlo simulations were designed so that the effect of scatter, attenuation, depth-dependent collimator response and finite spatial resolution could be studied individually and in combination. The impact of each physical effect and of combinations of effects was studied in terms of absolute and relative quantitative accuracy, spatial resolution and signal-to-noise ratio (SNR) in the resulting images. No corrections for these effects were assessed. Results obtained from Monte Carlo simulations and real acquisitions were in excellent agreement. Attenuation introduced about 90% activity underestimation in a 10-mm-thick left ventricle wall while finite spatial resolution alone introduced about 30% activity underestimation. Scatter had a negligible impact on quantitative accuracy in the recontructed slices when attenuation was present. Neither bull's eye map homogeneity nor contrast between a hot and a cold region were affected by depth-dependent collimator response or finite spatial resolution. Bull's eye map homogeneity was severely affected by attenuation but not by scatter. Attenuation and scatter reduced contrast by about 20% each. Both attenuation and scatter increased the full-width at half-maximum (FWHM) characterizing the spatial resolution of the imaging system by ≈ 1 mm each but the main effect responsible for the observed 11-mm FWHM spatial resolution was the depth-dependent collimator response. SNR was reduced by a factor of ≈ 2.5 because of attenuation, while scattered counts increased SNR by $\approx 10\%$. In conclusion, the quantification of the relative influence of the different physical effects showed that attenuation is definitely the major phenomenon affecting cardiac SPET imaging accuracy, but that finite spatial resolution, scatter and depth-dependent collimator response also contribute significantly to the errors in absolute and relative quantitation and to the poor spatial resolution.

Key words: Quantitation – Cardiac single-photon emission tomography – Monte Carlo simulation

Introduction

The accuracy of quantitation in single-photon emission tomography (SPET) is affected by many effects among which attenuation, scatter, depth-dependent collimator response and finite spatial resolution (FSR) play a major role. Studying the impact of each of these effects on the image characteristics (e.g. image resolution, relative and absolute quantitation, and signal-to-noise ratio) is necessary to determine what improvement could be expected if we were to perform an ideal correction for a given effect. However, these phenomena are not independent and each one should be considered only as a component responsible for part of the SPET system inaccuracies. Therefore, it is not sufficient to determine how each phenomenon taken independently affects the images. The impact of each phenomenon should also be characterized when it is combined with other phenomena affecting the imaging process, to determine the respective role of each phenomenon and the improvements that could be expected when correcting for some effects but ignoring the others.

Although many studies have been devoted to the investigation of the qualitative and quantitative conse-

Correspondence to: I. Buvat

quences of a single phenomenon such as scatter [e.g. 1–4], attenuation [e.g. 5–6] or depth-dependent collimator response [e.g. 7–10], or of the combination of two effects such as scatter and attenuation [11], the *respective* effect of each phenomenon in combination with others onto the image characteristics has not been thoroughly studied. The purpose of our investigation was therefore to determine the respective effect of scatter, attenuation, depth-dependent collimator response and FSR in cardiac SPET imaging so that the relative importance of the different corrections could be better predicted. An anthropomorphic cardiac phantom was considered because (1) all effects are a priori not negligible; (2) both image quality and quantitation are relevant in cardiac SPET. To permit a comprehensive investigation of how the phenomena affect the image characteristics, Monte Carlo simulations of the cardiac phantom were used.

Materials and methods

Phantom acquisitions

An anthropomorphic Data Spectrum cardiac phantom (Data-Spectrum, Chapel Hill, N.C.) was considered. The phantom consisted of an elliptical 24×32 cm cylinder, including a left ventricle (LV) compartment with a 10-mm-thick wall, two lung compartments filled with a mixture of expanded polystyrene and water, and a Teflon spine. A 530-ml perfusion bag was added to simulate the liver.

The LV and liver compartments were filled with a gadolinium solution, the lung and spine compartments were left unchanged, and the remainder of the phantom was filled with water. The phantom was scanned on an MRI scanner (SIGNA 1.5T-GE) using a 2D spin echo sequence (TR = 400 ms, TE = 200 ms) and a 256×256×124 volume was acquired (2.73×2.73×2 mm^3 voxels). The resulting images presented high signal intensity in the LV and liver compartments, intermediate signal intensity in the water-filled LV cavity and soft tissue compartments, and low signal intensity in the lungs and spine. Using thresholding operations, the images were segmented into regions corresponding to the lungs, LV wall, LV cavity, spine, liver and soft tissue. Each region was labelled so that the result of the segmentation could be used as an input for Monte Carlo simulations.

The phantom was then emptied. The LV compartment was removed and the LV wall was filled with 7.8 10^{-2} MBq/ml of technetium-99m. A SPET acquisition of this compartment alone was performed on a DST camera (SMVI, Buc, France) using a low-energy high-resolution (LEHR) collimator. Using a 20% energy window, 128 projections (60 s per projection) were acquired over a 360° circular orbit with a 20-cm radius of rotation. A total of 31.7 million events were acquired. The pixel size in the projections was 3.8×5 mm^2.

The LV compartment was then repositioned in the phantom. The liver was filled with 4.7 10^{-2} MBq/ml of ^{99m}Tc and the phantom was filled with water. A SPET acquisition using the same parameters as in the first SPET acquisition was performed, yielding a total of 2.3 million events detected in the 20% energy window projections. In addition, for this phantom, a planar acquisition corresponding to the anterior view was performed in list mode with energy information. For this planar acquisition, the centre of the phantom was at 20 cm from the collimator.

Monte Carlo simulation

The segmented images obtained from the MRI acquisition were used as an input for Monte Carlo simulations. The linear attenuation coefficients were assigned the narrow beam, energy-dependent values for lungs, bone, LV and soft tissues [12]. The Monte Carlo simulation software was based on SimSET [13] to which modelling of coherent scatter was added [14]. Scattered photons were tracked until the ninth order. Two simulations were performed to mimic the two SPET acquisitions. Three hundred and sixty million photons were simulated for each simulation. The first simulation was performed without any attenuating medium, as if the LV, liver and other tissues had the density of air, and resulted in 41 million photons detected in the 20% energy window projections (no variance reduction was used). The second simulation mimicked the SPET acquisition with liver and attenuating media. For this second simulation, variance reduction was used [13]. About 8 million photons were detected in the 20% energy projections. No Monte Carlo tracking of the photons was performed in the LEHR collimator and only the geometrical component of the collimator response was considered. The intrinsic energy response was modelled using Gaussian functions with standard deviation dependent on the energy (energy resolution set to 9.5% at 140 keV). For each simulation, 128 projections were simulated over a 360° circular orbit with a 20-cm radius of rotation. The Monte Carlo events were sorted depending on their energy, position (*x*, *y*, *z*) and nature (primary or scattered). The pixel size was 3.8×5 mm^2.

Data analysis

Evaluation criteria

Five criteria were considered to characterize the effects of the different phenomena: percent error between measured and true activity in regions of interest, uniformity of the bull's eye map (BEM), contrast between a hot and a cold region, spatial resolution and signal-to-noise ratio (SNR).

Percent error in activity. Percent errors in activity were calculated both in the simulated projections and in the slices reconstructed from the simulated and acquired data. In the simulated projections, they were computed with respect to the projections of primary photons only in LV and liver regions, to assess the effect of scatter. The LV ROI was obtained by considering the projection pixels with only LV activity in the primary projections (28 448 pixels in total), and the liver ROI was obtained by selecting the projection pixels in which there was only liver activity (91 539 pixels in total).

To calculate percent errors in activity in the reconstructed slices, the transverse slices were reoriented into short-axis slices and BEMs were derived. The BEMs were divided into nine myocardial regions (Fig. 1) and the mean activity in each region was calculated. Using the simulated data, the percent error in estimated LV wall activity compared with simulated activity or activity derived from the primary photon distribution only was calculated for each of the nine regions by comparing the mean estimated regional value with the reference regional value. The mean percent error over the nine regions was deduced. The percent error in estimated liver activity was measured in a ≈1000 voxel 3D ROI drawn inside the liver compartment.

To estimate the activity concentration using the acquired data, a cross-calibration factor (8 kcounts/pixel/MBq) was derived us-

Table 1. Evaluation strategy

Study	Comparing:	With:
1. Effect of scatter on the projections	20% window (I20) projections	Primary projections
2. Effect of scatter on the reconstructed slices	I20 projections + filtered backprojection (FBP) slices	Primary projections + FBP reconstructed slices
3. Effect of attenuation on the projections	Primary projections	Projections from the air simulation
4. Effect of attenuation on the reconstructed slices	Primary + FBP reconstructed slices	Air simulation + FBP reconstructed slices
5. Effect of depth-dependent collimator response	Air simulation + FBP reconstructed slices in the liver ROI	Reference activity in the liver
6. Effect of FSR	Air simulation + FBP reconstructed slices in the LV ROI	Air simulation + FBP reconstructed slices in the liver ROI
7. Effect of depth-dependent collimator response and FSR	Air simulation + FBP reconstructed slices in the LV ROI	Reference activity in the LV
8. Effect of scatter and attenuation	I20 projections + FBP reconstructed slices	Air simulation + FBP reconstructed slices
9. Effect of depth-dependent collimator response, FSR, attenuation and scatter	I20 projections + FBP reconstructed slices in the LV ROI	Reference activity in the LV

1. apical
2. lateral
3. anterior
4. septal
5. inferior
6. inferobasal
7. laterobasal
8. anterobasal
9. septobasal
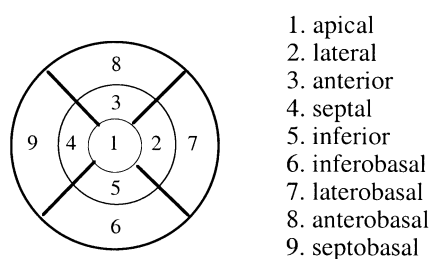
Fig. 1. The nine myocardial regions dividing the BEM

ing a point source SPET acquisition in air. The numbers of counts measured in the BEM or in a 3D liver ROI (≈1000 voxels) were converted into MBq/ml using this factor. The percent errors were calculated with respect to the true activity values in the LV wall and liver.

Uniformity of the bull's eye map. For each BEM derived from the reconstruction of the simulated or acquired data, the mean activity values in each of the nine BEM regions were normalized so that the highest of these nine values was 100. The mean of the nine normalized values defined a BEM uniformity index. As activity was uniformly distributed in the LV wall, the uniformity index should ideally be 100.

Contrast. For both the simulated and acquired data, the contrast was calculated between a 3D LV region (≈1000 voxels) drawn inside the LV wall activity distribution (≈2000 voxels) and a 3D LV cavity region (≈1000 voxels) drawn well inside the LV cavity of ≈3000 voxels. The mean numbers of counts m_1 and m_2 in these two regions were calculated and the contrast was defined as $(m_1-m_2)/(m_1+m_2)$. As there was no activity in the LV cavity, the ideal contrast should be 1.

Spatial resolution. Using the images reconstructed from the simulated or acquired data, each short-axis slice was normalized by multiplying each voxel value by the ratio of the total activity in the true 3D LV wall distribution to that in the reconstructed 3D LV distribution. This normalization removed the bias due to attenuation but did not modify the spatial distribution of counts. Each normalized short-axis slice was then divided into eight sectors and the radial count profile corresponding to each sector was calculat-

ed. Given the exact thickness of the wall (10 mm) and the theoretical uptake (7.8 10^{-2} MBq/ml), the profile that would be observed assuming a Gaussian response function with known full-width at half-maximum (FWHM) could be calculated. An optimization procedure [15] was used to determine the FWHM which minimized the mean square error between the predicted and the observed count profiles.

Signal-to-noise ratio. A 3D ROI (≈1000 voxels) was drawn inside the liver (total liver volume = ≈7500 voxels for the simulation and ≈6000 voxels for the acquisition) in which the activity was uniform. For each reconstruction from either the simulated or the acquired data, a Kolmogorov-Smirnov test [16] was performed to determine whether the voxel values in this ROI followed a Gaussian distribution. When this was the case, the SNR was calculated as the ratio of the mean over the standard deviation of the ROI voxel values.

Evaluation strategy

Using the simulated data, the effects of scatter and attenuation were first studied on the projections, then the effects of scatter, attenuation, depth-dependent collimator response and FSR were studied on the reconstructed volume, so that the propagation of the errors from projections to reconstructed slices could be determined. Using the reconstructed slices, each phenomenon was first studied alone. Then, the combination of some or all effects was investigated, to determine how each phenomenon or combination of phenomena contributed to the global quantitative error. Table 1 summarizes the comparison schemes. Each time it was possible, the figures obtained from the actual acquisition of the phantom were compared with those obtained from the simulations.

Analysis of the simulated projections

To study how scatter affected the projections, the 20% window (I20) simulated projections were compared with the primary photon projections.

The effect of attenuation was assessed by comparing the primary photons projections with the projections obtained with the same phantom in air.

Analysis of the reconstructed slices

In the following, filtered backprojection (FBP) using a Hann filter (cut-off frequency = 0.13 mm^{-1}) was always used for tomographic reconstruction.

Scatter. FBP reconstruction of the I20 and primary projections were compared in the LV and liver regions. The observed differences were due to scatter only.

Attenuation. The effect of attenuation only was characterized by comparing LV wall images reconstructed from the simulation in air (data affected by depth-dependent collimator response and FSR) with those reconstructed from the primary photons of the simulation with attenuating media (data affected by attenuation, depth-dependent collimator response and FSR) in the LV and liver regions.

Depth-dependent collimator response. The consequences of depth-dependent collimator response were investigated by comparing the activity distribution in the liver ROI after FBP reconstruction of the air data with the true liver activity, since the only phenomenon involved here was the depth-dependent collimator response. Although the LV is the clinically relevant region in cardiac imaging, the liver was considered because unlike the LV, it is not affected by partial volume effect resulting from FSR. Since only the LV compartment was acquired in air, the same comparison was not performed using the acquired data.

Finite spatial resolution. Even if the collimator response did not depend on the depth, FSR would cause partial volume effect in small structures such as the LV wall. To characterize the consequences of FSR alone, we assumed that the collimator response was only a function of the distance from the source to the collimator [17] and the validity of this assumption was checked. The error due to the depth-dependent collimator response in the LV was assumed to be identical to that measured in the liver, for LV and liver ROIs drawn at the same distance from the centre of rotation. The consequences of FSR alone were then deduced by comparing the errors observed when both depth-dependent collimator response and partial volume effect were involved (in the LV wall) with those observed when depth-dependent collimator response only affected the measurements (in the liver).

FSR and depth-dependent collimator response. The effect of depth-dependent collimator response combined with FSR on LV activity measurements was studied by comparing the LV wall activity measured from FBP reconstructed slices of the air projections with the true LV wall activity, for both the simulated and the acquired data.

Scatter and attenuation. The effect of scatter combined with attenuation was assessed by comparing the I20 + FBP LV reconstruction with the air + FBP LV reconstruction for both simulated and acquired data. Since reconstructed slices were affected identically by depth-dependent collimator response and FSR, the observed differences were due to scatter in the I20 window and attenuation in the non-uniform attenuating media.

Scatter, attenuation, FSR and depth-dependent collimator response. Using both the acquired and the simulated data, the consequences of all combined effects were characterized by comparing the FBP reconstruction of the I20 projections with the true activity in the LV.

Results

Projections

Scatter. The energy spectra corresponding to the acquired data and to the simulated anterior projection were compared (Fig. 2a) and showed close agreement, except below 85 keV because the X-ray radiations resulting
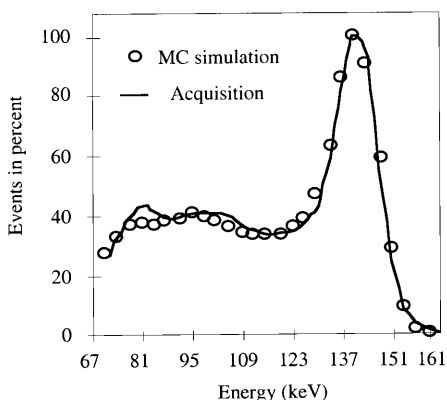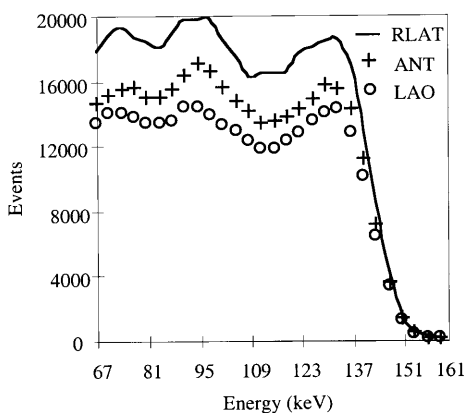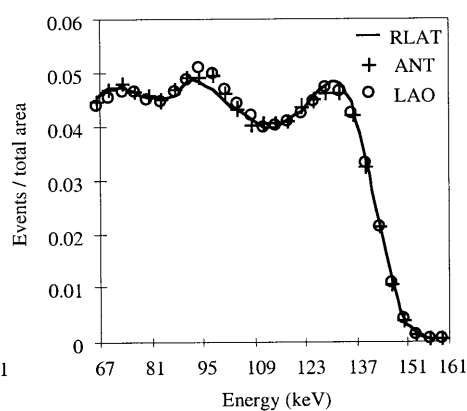
Fig. 2a–c. a Acquired (–) and simulated (○) spectra for the anterior projection. **b** Simulated scatter spectra for the right lateral projection (–), the anterior projection (+) and the left anterior oblique projection (○). **c** Same as **b** but with spectra normalized to the same area

from the gamma interactions with the lead of the collimator were not simulated. The ratio of the primary to the total number of photons in the 20% energy window varied between 53% for the right lateral projection (RLAT) and 62% for the left anterior oblique projection (LAO). As expected, the primary spectrum was identical in shape for all projections but varied in area from 40 000 primary photons in the RLAT projection to 163 000 primary photons in the LAO projection. The total scatter spectra (from 63 to 161 keV) over each projection also varied in area from 133 600 scattered photons in the left lateral and LAO projections to 405 000 scattered photons in the RLAT projection, and varied only slightly in shape (Fig. 2b,c). The number of photons in the I20 images overestimated the true number of primary photons by 56% (anterior view) to 75% (LAO) (mean = 60%±10%). The true number of primary photons was overestimated by 46%±14% and 47±11% in the LV and liver regions respectively.

Attenuation. The impact of attenuation alone was assessed by comparing the activity in the LV and liver ROIs for the primary photon projections with the activity in the LV and liver ROIs for the projections resulting from the air simulation. The LV activity underestimation varied from 97% in the right posterior oblique (RPO) and RLAT projections to 83% in the LAO projection (mean = 89%±5%). The liver activity underestimation varied between 98% in the LAO projection and 76% in the RPO projection (mean = 87%±8%).

Reconstructed slices

Scatter. The percent errors with respect to the primary photon activity distribution in the LV and liver ROIs are shown in the first column of Table 2. For the LV region, the percent error due to scatter was smaller in the reconstructed slices (20%±5% in I20 + FBP) than in the projections (46%±14% in the I20 projections) (*t* test, *P*<0.05). The same trend was observed for the liver region: 23%±4% in the I20 + FBP images against 47%±11% in the I20 projections (*P*<0.05). Table 3 shows that scatter did not affect BEM homogeneity: 78%±14% in the I20 + FBP image as compared with 79%±14% in the primary BEM (NS). Scatter had little effect on spatial resolution as measured by the FWHM of the imaging system point spread function: FWHM was 13±1 mm with I20 + FBP as compared with 12±1 mm with primary + FBP slices (NS). Kolmogorov-Smirnov tests showed that the voxel values in the liver ROI followed a Gaussian distribution for I20 + FBP, primary + FBP and air + FBP slices. SNR, defined by the ratio of the mean to the standard deviation of the ROI voxel values, was slightly higher when scattered photons were included (4.7 in the I20 + FBP slices compared with 4.3 in the primary + FBP slices). Finally, scatter reduced contrast between the LV cavity and the LV wall

Table 2. Quantitative errors in the LV and liver ROIs obtained from the simulated data (first row in each cell, normal characters) and, when available, from the acquired data (second row in each cell, italic characters)

LV ref = 380 counts Liver ref = 222 counts	Error with respect to primary reconstruction	Error with respect to air reconstruction	Error with respect to the reference
Air +FBP (LV)	–	–	–34±2
	–	–	*–38±2*
Air +FBP (liver)	–	–	–5±1
	–	–	–
Primary + FBP (LV)	–	–89±3	–93±1
	–	–	–
Primary + FBP (liver)	–	–88±2	–89±1
	–	–	–
I20 + FBP (LV)	20±5	–87±2	–91±2
		–89±2	*–93±3*
I20 + FBP (liver)	23±4	–88±2	–86±1
	–	–	*–89±2*

Table 3. BEM homogeneity, resolution, SNR and contrast in the reconstructed images obtained from the simulated data (first row in each cell, normal characters) and, when available, from the acquired data (second row in each cell, italic characters)

	Homogeneity (%)	Resolution (mm)	SNR	Contrast
I20 + FBP	78±14	13.0±1.1	4.7	0.60
	72±13	*13.5±1.2*	*4.8*	*0.68*
Primary + FBP	79±14	12.2±1.0	4.3	0.73
	–	–	–	–
Air + FBP	96±3	11.5±0.9	10.6	0.96
	94±5	*12.1±1.1*	*9.8*	*0.90*

(Table 3), from 0.73 in the primary + FBP reconstruction to 0.60 with I20 + FBP.

Attenuation. The quantitative error due to attenuation was assessed by comparing the LV activity in the FBP reconstruction of the primary photons (from the simulation with attenuating media) with the FBP reconstruction of the air simulation (Fig. 3). The LV activity was reduced by 89%±3% (Table 2) as a consequence of attenuation only. A similar activity underestimation (88%±2%) was observed in the liver ROI. Attenuation also had a severe effect on BEM homogeneity (Table 3), which dropped from 96%±3% for the air simulation to 79%±14% for primary + FBP BEM (*P*<0.05). Attenuation did not affect spatial resolution significantly: 12±1 mm for the primary + FBP slices compared with 11±1 mm in the air + FBP slices (NS). SNR decreased dramatically because of attenuation from 10.6 in the air + FBP reconstruction to 4.3 in the primary + FBP recon-
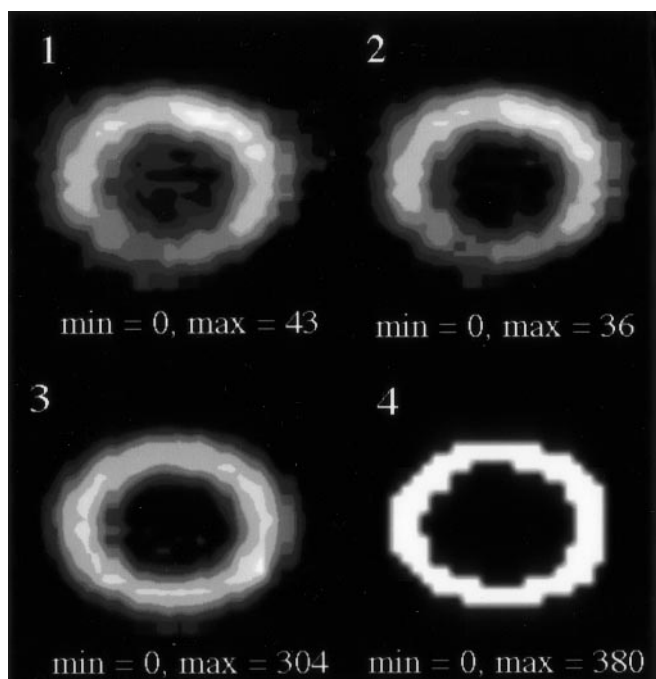
Fig. 3. Short-axis images corresponding to I20 + FBP (*1*), primary + FBP (*2*), air + FBP (*3*) and reference activity distribution (*4*)

struction. Attenuation also had a deleterious effect on contrast between the LV wall and LV cavity: 0.73 for the primary + FBP reconstruction against 0.96 for the air + FBP reconstruction.

Depth-dependent collimator response. In the air + FBP reconstruction of the simulated data, the liver activity was underestimated by 5%±1% compared with the liver reference activity (Table 2). As there were no scatter, no attenuation and no partial volume effect, this underestimation is due to the variable resolution of the collimator response and/or the imperfections of the reconstruction algorithm.

FSR. To investigate the consequences of partial volume effect resulting from FSR, it was first verified that the effect of the collimator response was only a function of the distance between the source and the centre of rotation (COR) of the gamma camera. Using the simulated data, seven ROIs were drawn in different liver regions of the air + FBP reconstructed slices at 2.7 cm from the COR and 16 ROIs were drawn at a distance of 9.8 cm. The liver activity was underestimated by 3.4% ±0.1% at 2.7 cm and by 4.7%±0.2% at 9.8 cm, showing that although the error depended on the distance from the COR, it was almost constant at a given distance from the COR. The error in the LV wall activity in seven LV ROIs located at 2.7 cm from the COR was –34%±1% while the error in eight LV ROIs located at 9.8 cm was –36%±2%. It was then deduced that the underestimation of activity distribution in the LV due to partial volume effect alone was approximately 31%–32%.

FSR and depth-dependent collimator response. The combined effect of partial volume effect resulting from FSR and depth-dependent collimator response was assessed by comparing the air + FBP slices with the LV reference activity distribution (Fig. 3). Considering the simulated data, the LV activity was underestimated by 34%±2% (Table 2). Homogeneity was 96%±3% in air + FBP BEM as compared with 100% in the reference BEM (Table 3). Resolution was 11±1 mm in air + FBP. This value can be compared with the spatial resolution measured using a point source located at a distance from the collimator equal to that of the LV wall region used to measure spatial resolution (18.4 cm), which was 11.8 mm. SNR was 10.6 and contrast was 0.96. For all indices, very close values were obtained using the images corresponding to the actual acquisition of the LV compartment in air (values in italics in Table 3).

Scatter and attenuation. The combined effect of scatter and attenuation was assessed by comparing the I20 + FBP slices with the air + FBP slices (Fig. 3). Using the simulated data, the LV activity measured from the I20 + FBP slices was underestimated by 87%±2% compared with the activity measured on the air + FBP volume (Table 2), while the corresponding underestimation was 88%±2% in the liver. BEM homogeneity (Table 3) fell from 96%±3% with air + FBP slices to 78%±14% ($P<0.05$) with I20 + FBP. Spatial resolution was 13±1 mm in the I20 + FBP slices as compared with 11±1 mm in the air + FBP slices ($P<0.05$). SNR and contrast were severely reduced because of scatter and attenuation (SNR = 4.7 in I20 + FBP images as compared with 10.6 in the air + FBP images; contrast = 0.60 in I20 + FBP as compared with 0.96 in the air + FBP slices). Similar to what was observed for the air data, in the I20 + FBP reconstruction of data affected by attenuation, the values of the indices measured from the slices reconstructed using the acquired data were very close to the values measured from the slices reconstructed using the simulated data (Table 3, values in italics).

Scatter, attenuation, FSR and depth-dependent collimator response. When all effects were introduced (scatter, attenuation, depth-dependent collimator response and FSR), the LV activity was underestimated by 91%±2% in the simulations (Table 2). In the liver ROI which was not affected by partial volume effect, the activity underestimation was 86%±1%. The BEM homogeneity dropped from a theoretical value of 100% to only 78%±14% because of all combined effects (Table 3). Spatial resolution was 13±1 mm in the I20 + FBP slices. Both SNR and contrast were low (SNR = 4.7 and contrast = 0.60). Again, the values measured on the images resulting from the real acquisition were very close to those obtained from the simulations (Table 3, values in italics). These image characteristics would typically be what one would observe when cardiac images are reconstructed without any correction.

Discussion

It is well known that attenuation, scatter, depth-dependent collimator response and FSR all affect SPET imaging. However, the relative impact of each of these effects on the different image characteristics is not yet completely understood. For investigating the respective role of the different effects, Monte Carlo simulations were used to reproduce imaging conditions close to those encountered in clinical practice while controlling exactly all parameters and photon histories. Monte Carlo simulations must be carefully validated before they can be trusted and used to reproduce realistic configurations. Our simulation was therefore performed using a cardiac phantom with a realistic anatomical shape, for which real acquisitions could be performed for comparison. In addition to other validation tests of the simulation code previously performed, the data simulated for this paper were validated by comparing the spectrum corresponding to a given simulated projection with the corresponding spectrum acquired on a gamma camera. Furthermore, whenever possible, the values of indices measured using the simulated data were compared with those measured from the corresponding acquired data. In all instances, close agreement between simulated and acquired data was found, confirming that the simulations can certainly provide realistic information regarding the relative influence of the different factors affecting SPET cardiac imaging.

Absolute quantitation

The phenomenon affecting absolute quantitation the most was attenuation. Comparing simulations with and without attenuating media, attenuation reduced the activity by 88% in both projections and reconstructed slices for the LV and the liver ROIs. In the projections, this error varied more in the liver ROI than in the LV ROI because the LV was smaller and closer to the COR of the camera than the liver. The quantitative error was similar in the projections and in the reconstructed slices. The underestimation observed in the reconstructed slices is consistent with Almquist et al.'s results [18] for hot point sources located in different attenuating media at equivalent depth: an 81% underestimation was observed with respect to the activity measured in air when no corrections were performed.

The second phenomenon which greatly affected absolute quantitation in the LV was partial volume effect resulting from FSR. For a 10-mm-thick wall (roughly corresponding to the end diastole thickness in a patient), partial volume effect caused by FSR and depth-dependent collimator response resulted in an activity underestimation greater than 30%. These results are in agreement with those obtained by Buvat et al. [19] using a square wave model (30% activity underestimation due to partial volume effect alone for a wall thickness of

10 mm and a resolution of 11 mm). This is also consistent with the 28% underestimation measured by Galt et al. [9] in a cardiac phantom for a wall thickness to FWHM ratio equal to 1 and with the 25% underestimation reported by Kojima et al. [7] for a hot cylinder embedded in water with a cylinder diameter equal to the FWHM. For large objects in which partial volume effect is not of concern, such as the liver in our phantom, absolute quantitation was quite accurate (error <5%) when there was no attenuation nor scatter. Kojima et al. [7] also obtained a recovery coefficient of 1 when the activity was measured in hot cylinders with a diameter greater than 3 times the FWHM. This suggests that, for large objects, there is no need of depth-dependent collimator response and partial volume effect corrections but absolute quantitation would be accurate with perfect attenuation and scatter corrections. On the other hand, accurate absolute quantitation of the LV wall activity definitely requires partial volume effect and depth-dependent collimator response corrections, in addition to attenuation and scatter corrections.

Scatter also affects quantitation. In the projections, the influence of scatter strongly depended on the view. When investigating how the quantitative error due to scatter only propagates from the projections to the reconstructed slices using FBP reconstruction without attenuation correction, it was found that an activity overestimation of about 45% in the projections reduced to about 20% after reconstruction. Therefore, when no attenuation correction is performed, the deleterious quantitative effect of scatter is greater in the projections than in the reconstructions. This is because more scattered than unscattered photons are attenuated as the attenuation coefficient increases with decreasing energy. Consequently, the ratio of unscattered to scattered photons is higher in the reconstructed slices than in the projections. This observation also explains why, when assessing a scatter correction method, the impact of the correction is greater on the projections than on the reconstructed slices, when no attenuation correction is associated with the scatter correction [20]. Note that this propagation of error would certainly be different had the reconstruction algorithm included an attenuation correction. With attenuation, the effect of scatter on absolute quantitation was negligible, i.e. the quantitative error was dominated by attenuation (89% LV activity underestimation when considering the primary photons and 86% underestimation when considering the I20 photons). In other words, for absolute quantitation, there is no point in correcting for scatter if attenuation is not corrected for.

In summary, for a 10-mm-thick wall where the true value is 100 photons given the sensitivity of the camera, only ≈9 photons would be detected. Among these nine photons, there would be two scattered photons. Using perfect attenuation and scatter corrections, 66 photons would be restored instead of 100, i.e., attenuation correction applied on scatter-free images should result in a ≈9 times enhancement of the LV activity. The gap between

66 and 100 shows that partial volume effect should definitely be corrected for to restore the true LV wall activity. The observed activity might have to be multiplied by as much as 1.5 for a 10-mm-thick wall to estimate the true underlying activity. Liver measurements showed that assuming partial volume effect could be perfectly corrected for, absolute activity could be accurately estimated within 5%. In other words, using partial volume effect correction combined with scatter and attenuation corrections should restore more than 95 photons. While attenuation and scatter corrections are currently in the stage of clinical evaluation [18, 21–24], partial volume effect correction is not yet available for cardiac SPET, and should certainly now be considered to achieve accurate LV activity quantitation [9].

Relative quantitation

Relative quantitation was studied by analysing BEMs and contrast values. While BEM homogeneity characterizes relative quantitation between several equally hot regions, the calculated contrast characterizes relative quantitation between the hot LV wall and the cold LV cavity. BEM homogeneity was mostly affected by attenuation. With FSR and depth-dependent collimator response effect only, BEM homogeneity was 96%±3%, i.e., very close to the ideal 100% homogeneity. This shows that for a 360% acquisition where the LV is very close to the COR, a correction for the depth-dependent collimator response should not significantly affect BEM homogeneity. Attenuation reduced homogeneity to 79%±14%. Attenuation and scatter did not change homogeneity with respect to attenuation only (78%±14%). These results agree with the homogeneity computed for the BEM given by Luo et al. [25] which was 98% in air for the MCAT LV phantom and 82% with attenuation and scatter. Unlike attenuation, neither scatter nor FSR nor depth-dependent collimator response affect BEM homogeneity much for a uniform LV wall activity. This could explain why homogeneity of tracer distribution improved after attenuation correction only for patients with low likelihood of coronary artery disease [21]. It has been shown that scatter may affect BEM homogeneity [5, 21, 25] when the liver is close enough to the LV. In our phantom, the minimum distance between a liver point and an LV point was about 9 cm and we did not observe an effect of scatter upon BEM homogeneity. We conclude that for scatter to perturb BEM map homogeneity, liver and LV should be less than 9 cm apart. However, a safe approach should consist in correcting for both scatter and attenuation before evaluating BEM homogeneity to avoid artifacts [5, 21].

Unlike BEM homogeneity, contrast between a hot and a cold region was significantly affected by both attenuation and scatter. With FSR and depth-dependent collimator response only, contrast was 0.96, very close to the ideal contrast of 1. In agreement with the results

obtained when studying BEM homogeneity, this confirms that partial volume effect and depth-dependent collimator response corrections are therefore probably not required to improve relative quantitation in 360° cardiac SPET when the heart is close to the COR, as in our phantom. This is consistent with the result of Ye et al. [26], who obtained an improvement of only 2% of the basal to apical activity ratio in a cardiac Data Spectrum phantom when depth-dependent collimator response correction was added to attenuation correction. Attenuation decreased the contrast to 0.73, while attenuation and scatter reduced it to 0.60. Therefore, both scatter and attenuation should be corrected for to improve contrast.

The reduction of contrast caused by attenuation is consistent with the results regarding BEM homogeneity. Attenuation reduces counts by different amounts depending on the location of the regions, and therefore results in a bias when calculating the ratio between two hot regions (as measured by BEM homogeneity) or between a hot and a cold region (as measured by contrast). The reason why scatter reduced contrast without affecting BEM homogeneity is as follows: when considering a region uniformly hot (the LV wall in our phantom), in a given ROI1, scattered counts coming from adjacent regions balance counts from ROI1 which scatter and escape from ROI1. On the other hand, when considering a cold region, scattered photons come from outside but no photon leaves the cold region: there is therefore no equilibrium between incoming and escaping photons. As a result, relative quantitation between two equally hot regions is not affected by scatter, while relative quantitation between a cold and a hot region or two hot regions containing different amounts of activity is. These results allow us to predict the effect of scatter upon BEM homogeneity when perfusion defects are present: by reducing contrast between cold and hot regions, scatter would artefactually increase BEM homogeneity when activity is intrinsically non-uniform in the LV wall. This suggests that when looking for perfusion defects in cardiac imaging, both attenuation and scatter should be compensated.

Spatial resolution

The FWHM of the imaging system point spread function was used to characterize spatial resolution. The FWHM measured without attenuation nor scatter (11.5 mm) was consistent with the FWHM characterizing the collimator response (11.8 mm) for the corresponding LV wall-collimator distance (184 mm), confirming that partial volume effect does not affect spatial resolution. It can therefore be expected that the correction which should improve spatial resolution the most is the depth-dependent collimator response correction [27–29]. Such a correction should contribute to fill the gap between the 11.5 mm resolution observed without scatter or attenuation and the ≈5 mm corresponding to the intrinsic response of a

gamma camera. Formiconi et al. [30] actually reported a 6-mm improvement (from 15 mm to 9 mm) when including compensation of variable collimator response in the iterative conjugate gradient reconstruction algorithm. Scatter and attenuation corrections should only have a small impact on spatial resolution improvement compared with that of depth-dependent collimator response correction (FWHM increased by 1 mm and 0.7 mm due to scatter and attenuation respectively). The observed 6% loss of resolution due to scatter is consistent with the results of Beck et al. [1], who found a 5% improvement of the FWHM in line sources at a comparable depth in water after scatter correction. The 6% loss of resolution due to attenuation is also in agreement with the findings of Manglos et al. [6], who reported a <5% improvement in resolution when attenuation correction was performed for a linear source centrally located in an elliptical torso phantom of dimensions similar to those of our phantom.

Signal-to-noise ratio

SNR is a critical parameter for lesion detection. SNR measurements in a liver region with Gaussian count distribution showed that the phenomenon which affects SNR the most was attenuation. Because of the severe loss of counts due to attenuation, SNR was dramatically reduced from 10.6 to 4.3. By restoring counts, attenuation correction could therefore significantly increase SNR. SNR was slightly higher in the images including scattered photons (I20 + FBP) compared with images including primary photons only. This is because the larger the number of counts (scatter or primary), the greater the SNR. As a result, scatter corrections which remove (as opposed to relocate) scattered photons should intrinsically deteriorate SNR, as has been previously found [31, 32]. Further studies need to be performed to assess the role of variable collimator response correction on SNR [33].

Using our results, Table 4 gives indications regarding which corrections should be performed in order of priority depending on the image feature of interest, and also summarizes the performance that might be expected. These recommendations have been derived from a specific cardiac imaging situation, considering a static cardiac phantom and assuming accurate correction methods would be available. As a result, they should certainly not be considered as ground truth but should only be viewed as an insight into what the respective role of different corrections is expected to be in a typical situation of cardiac imaging. The effect of changes in patient-related parameters (such as addition of breast, larger body habitus, presence of perfusion defects) and heart motion will be considered in future work to determine how variable the respective influence of the different phenomena might be. However, the italicized characters in Table 4 indicate the conclusions that are the most likely to remain valid in cardiac imaging in general, whatever the patient-specific features. On the other hand, further bib-

Table 4. Expected role of the different corrections in cardiac imaging

	Absolute quantitation of the LV wall activity	Spatial resolution (FWHM)	Bull's eye map homogeneity	Contrast between a hot and a cold region	Signal-to-noise ratio
Priority 1	ATTENUATION CORRECTION	DEPTH-DEPENDENT COLLIMATOR RESPONSE CORRECTION	ATTENUATION CORRECTION	SCATTER CORRECTION	ATTENUATION CORRECTION
	If not, activity underestimation of ≈90%	*If not, expected ≈11 mm spatial resolution. With correction, ≈6 mm resolution could be expected*	*Definitely required*	*Expected significant contrast increase (≈20%)*	*Possible SNR increase by a factor >2*
Priority 2	PARTIAL VOLUME EFFECT (PVE) CORRECTION	SCATTER CORRECTION	SCATTER CORRECTION	ATTENUATION CORRECTION	DEPTH-DEPENDENT COLLIMATOR RESPONSE CORRECTION
	If not, activity underestimation of ≈30% for 10-mm-thick wall	*Little effect (≤1 mm gain in FWHM)*	Should be performed if high liver activity and low liver-LV distance	*Expected significant contrast increase (≈20%)*	?
Priority 3	SCATTER CORRECTION	ATTENUATION CORRECTION	DEPTH-DEPENDENT COLLIMATOR RESPONSE CORRECTION	Depth-dependent collimator response correction	Scatter correction subtraction methods will reduce SNR
	To avoid ≈20% activity overestimation	*Little effect (≤1 mm gain in FWHM)*	Negligible effect	Small positive effect as a result of spatial resolution improvement	Repositioning methods could improve it ?
Priority 4	DEPTH-DEPENDENT COLLIMATOR RESPONSE CORRECTION	PVE CORRECTION	PVE CORRECTION	PVE CORRECTION	PVE CORRECTION
	Not necessary, provided heart is near COR	*Definitely useless*	*Definitely useless*	*Definitely useless*	*Definitely useless*

liographic and experimental studies are in progress to determine whether available correction methods actually result in the theoretically expected performance.

References

1. Beck JW, Jaszczak RJ, Starmer CF. The effect of Compton scattering on quantitative SPECT imaging. In Raynaud C, ed. *Proceedings of the Third World Congress of Nuclear Medicine and Biology.* Paris: Pergamon Press; 1982: 1042–1045.

2. Floyd CE, Jaszczak RJ, Harris CC, Coleman RE. Energy and spatial distribution of multiple order Compton scatter in SPECT: a Monte Carlo investigation. *Phys Med Biol* 1984; 29: 1217–1230.

3. Szabo Z, Links JM, Seki C, Rhine J, Wagner HN. Scatter, spatial resolution, and quantitative recovery in high resolution SPECT. *J Comput Assist Tomogr* 1992; 16: 461–467.

4. Gagnon D, Laperrière L, Pouliot N, De Vries DJ, Moore SC. Monte Carlo analysis of camera-induced spectral contamination for different primary energies. *Phys Med Biol* 1992; 37: 1725–1739.

5. King MA, Tsui BMW, Pan TS. Attenuation compensation for cardiac single-photon emission computed tomographic imaging: Part 1. Impact of attenuation and methods of estimating attenuation maps. *J Nucl Cardiol* 1995; 2: 513–524.

6. Manglos SH, Jaszczak RJ, Floyd CE, Hahn LJ, Greer KL, Coleman RE. Nonisotropic attenuation in SPECT: phantom tests of quantitative effects and compensation techniques. *J Nucl Med* 1987; 28: 1584–1591.

7. Kojima A, Matsumoto M, Takahashi M, Hirota Y. Effect of spatial resolution on SPECT quantification values. *J Nucl Med* 1989; 30: 508–514.

8. Knesaurek K, King MA, Glick SJ, Penney BC. Investigation of causes of geometric distortion in 180° and 360° sampling in SPECT. *J Nucl Med* 1989; 30: 1666–1675.

9. Galt JR, Garcia EV, Robbins WL. Effects of myocardial wall thickness on SPECT quantification. *IEEE Trans Med Imaging* 1990; 9: 144–150.

10. Zito F, Gilardi MC, Magnani P, Fazio F. Single-photon emission tomographic quantification in spherical objects: effects of object size and background. *Eur J Nucl Med* 1996; 23: 263–271.

11. Beck JW, Jaszczak RJ, Coleman RE, Starmer CF, Nolte LW. Analysis of SPECT including scatter and attenuation using sophisticated Monte-Carlo modeling methods. *IEEE Trans Nucl Sci* 1982; 29: 506–511.

12. Picard Y, Thompson CJ, Marrett S. Improving the precision and accuracy of Monte Carlo simulation in positron emission tomography. *IEEE Trans Nucl Sci* 1992; 39: 1111–1116.

13. Harrison RL, Vannoy SD, Haynor DR, Gillispie SB, Kaplan MS, Lewellen TK. Preliminary experience with the photon history generator module of a public-domain simulation system for emission tomography. *Conf Rec Nucl Sci Symp* 1993; 2: 1154–1158.

14. El Fakhri G. *Evaluation pour la quantification en tomographie d'émission monophotonique.* Thèse de Doctorat, Université de Paris XI, 1998.

15. Powell MJD. An efficient method for finding the minimum of a functional of several variables without calculating derivatives. *Computer J* 1964; 7: 155–162.

16. Siegel S, Castellan NJ. *Nonparametric statistics for the behavioral sciences.* New York, 1988.

17. Metz CE, Atkins FB, Beck RN. The geometric transfer function component for scintillation camera collimators with straight parallel holes. *Phys Med Biol* 1980; 25: 1059–1070.

18. Almquist H, Palmer J, Ljungberg M, Wollmer P, Strand SE, Jonson B. Quantitative SPECT by attenuation correction of the projection set using transmission data: evaluation of a method. *Eur J Nucl Med* 1990; 16: 587–594.

19. Buvat I, Bartlett ML, Kitsiou AN, Dilsizian V, Bacharach SL. A "hybrid" method for measuring myocardial wall thickening from gated PET/SPECT images. *J Nucl Med* 1997; 38: 324–329.

20. McCool D, Barlow R, Buscombe J, Agnew J. Evaluation of SPECT for scintimammography using a novel breast phantom. *Eur J Nucl Med* 1998; 25: 911.

21. Prvulovitch EM, Lonn AH, Bomanji JB, Jarritt PH, Ell PJ. Effect of attenuation correction on myocardial Thallium-201 distribution in patients with a low likelihood of coronary artery disease. *Eur J Nucl Med* 1997; 24: 266–275.

22. King MA, Glick SJ, Penney BC. Activity quantitation in SPECT: a comparison of three attenuation correction methods in combination with pre-reconstruction restoration filtering. *IEEE Trans Nucl Sci* 1991; 38: 755–760.

23. Bonnin F, Buvat I, Benali H, Di Paola R. A comparative study of scatter correction methods for scintigraphic images. *Eur J Nucl Med* 1994; 21: 388–393.

24. Ljungberg M, King MA, Hademenos GJ, Strand SE. Comparison of four scatter correction methods using Monte Carlo simulated source distributions. *J Nucl Med* 1994; 35: 143–151.

25. Luo D, King MA, Morgan HT, et al. Investigations into possible causes of hot inferior wall artifacts in attenuation corrected cardiac perfusion images. *IEEE Trans Nucl Sci* 1997; 44: 1146–1153.

26. Ye J, Liang Z, Harrington DP. Quantitative reconstruction for myocardial perfusion SPECT: an efficient approach by depth-dependent deconvolution and matrix rotation. *Phys Med Biol* 1994; 39: 1263–1279.

27. Lewitt RM, Edholm PR, Xia W. Fourier method for correction of depth-dependent collimator blurring. *SPIE* 1989; 1092: 232–243.

28. Zeng GL, Gullberg GT. Frequency domain implementation of the three-dimensional geometric point response correction in SPECT imaging. *IEEE Trans Nucl Sci* 1992; 39: 1444–1453.

29. Xia W, Lewitt RM, Edholm PR. Fourier correction for spatially variant collimator blurring in SPECT. *IEEE Trans Med Imaging* 1995; 14: 100–115.

30. Formiconi AR, Pupi A, Passeri A. Compensation of spatial system response in SPECT with conjugate gradient reconstruction technique. *Phys Med Biol* 1989; 34: 69–84.

31. Buvat I, Rodriguez-Villafuerte M, Todd-Pokropek A, Benali H, Di Paola R. Comparative assessment of nine scatter correction methods based on spectral analysis using Monte Carlo simulations. *J Nucl Med* 1995; 36: 1476–1488.

32. Narita Y, Iida H, Eberl S, Nakamura T. Monte Carlo evaluation of accuracy and noise properties of two scatter correction methods for ^{201}Tl cardiac SPECT. *IEEE Trans Nucl Sci* 1997; 44: 2465–2472.

33. Hutton BF, Hudson HM, Beekman FJ. A clinical perspective of accelerated statistical reconstruction. *Eur J Nucl Med* 1997; 24: 797–808.